PHILOSOPHICAL TRANSACTIONS OF THE ROYAL SOCIETY A MATHEMATICAL, PHYSICAL & ENGINEERING SCIENCES

Physics of Melt Extraction: Theory, Implications and Applications

Marc Spiegelman

Phil. Trans. R. Soc. Lond. A 1993 **342**, 23-41
doi: 10.1098/rsta.1993.0002

Physics of melt extraction: theory, implications and applications

By Marc Spiegelman

Lamont-Doherty Geological Observatory, of Columbia University, Palisades, New York 10964, U.S.A.

This paper presents a general overview of flow in deformable porous media with emphasis on melt extraction processes beneath mid-ocean ridges. Using a series of simple model problems, we show that the equations governing magma migration have two fundamentally different modes of behaviour. Compressible two-phase flow governs the separation of melt from the solid and forms a nonlinear wave equation that allows melt to propagate in solitary waves. Incompressible two-phase flow governs small-scale mantle convection driven by lateral variations in melt content. The behaviour of both compressible and incompressible matrix deformation is demonstrated in the context of mid-ocean ridges to show that both mechanisms may explain the observation of the narrowness of ridge volcanism. These results also suggest that melt extraction is an inherently time dependent process that may account for the timing, volume and chemistry of volcanism.

1. Introduction

Magma migration and other important geophysical two-phase flows have long been considered to be efficient processes for transporting heat and mass in the mantle and the crust. However, it is only with the derivation of a comprehensive system of conservation equations (McKenzie 1984; Scott & Stevenson 1984, 1986; Fowler 1985) that we have begun to understand the fluid mechanics of these processes. The purpose of this paper is to develop a better physical understanding of the behaviour of two-phase flows through a series of simple model problems. Section 2*a* reviews the general equations governing viscous two-phase flows and presents some model problems to demonstrate that magma migration is an inherently time-dependent process. Section 3 then illustrates the behaviour of the governing equations in a more geological context to understand some of the possible processes involved in melt extraction at mid-ocean ridges. Given a better understanding of the general physics, the geological implications of these problems becomes clear and we can begin to use this insight to design experiments to test the theory and use observations to reveal the properties of the partly molten mantle.

2. General physics

(*a*) *Governing equations*

The equations governing the percolative flow of a low viscosity fluid or 'melt' through a viscously deformable permeable matrix were derived independently by several workers (McKenzie 1984; Scott & Stevenson 1984, 1986; Fowler 1985) based

Phil. Trans. R. Soc. Lond. A (1993) **342**, 23–41
Printed in Great Britain

on the more general work of Drew (1971, 1983) for interpenetrating two-phase flows. Of these formulations, McKenzie (1984) provides a particularly detailed derivation and is perhaps the more general. These equations are a macroscopic description of two interpenetrating viscous fluids with vastly different viscosities. The melt is assumed to form an interconnected porous network distributed over some characteristic pore (or vein spacing) a. As a continuum approximation, these equations are valid for length scales much larger than a and smaller than any characteristic variation in porosity. These equations also assume that inertial effects are negligible for both the percolating melt phase and for creeping matrix deformation. This assumption should remain valid as long as the porosity is much smaller than the critical value at which the matrix disaggregates.

With these considerations, the equations governing conservation of mass and momentum can be written

$$\partial(\rho_{\mathrm{f}}\phi)/\partial t+\nabla\cdot(\rho_{\mathrm{f}}\phi\boldsymbol{v})=\Gamma, \tag{1}$$

$$\partial[\rho_{\mathrm{s}}(1-\phi)]/\partial t+\nabla\cdot[\rho_{\mathrm{s}}(1-\phi)\,\boldsymbol{V}]=-\Gamma, \tag{2}$$

$$\phi(\boldsymbol{v}-\boldsymbol{V})=(-k_\phi/\mu)\nabla\mathscr{P}, \tag{3}$$

$$\frac{\partial\mathscr{P}}{\partial x_i}=\frac{\partial}{\partial x_j}\eta\left(\frac{\partial V_i}{\partial x_j}+\frac{\partial V_j}{\partial x_i}\right)+\frac{\partial}{\partial x_i}(\zeta-\tfrac{2}{3}\eta)\nabla\cdot\boldsymbol{V}-(1-\phi)\,\Delta\rho g\delta_{i3}, \tag{4}$$

$$k_\phi\sim a^2\phi^n/b. \tag{5}$$

In (1)–(5), ρ_{f} is the density of the melt, ϕ is the volume fraction occupied by the melt or porosity, $\boldsymbol{v}$ is the melt velocity, and Γ is the rate of mass transfer from matrix to melt (melting rate). ρ_{s} is the density of the solid matrix, $\boldsymbol{V}$ is the matrix velocity, k_ϕ is the permeability, μ is the melt viscosity and $\mathscr{P}=P-\rho_{\mathrm{f}}gz$ is the pressure in excess of hydrostatic pressure. $\mathscr{P}$ is often referred to as the 'piezometric pressure', or 'hydraulic head'. η and ζ are respectively, the matrix shear and bulk viscosities and $\Delta\rho=\rho_{\mathrm{s}}-\rho_{\mathrm{f}}$. Estimates and explanations of additional parameters are given in table 1.

Equations (1) and (2) conserve mass for the melt and matrix individually but allow mass transfer between solid and liquid via the melting rate Γ. If Γ is positive the solid melts. $\Gamma<0$ implies freezing. Equation (3) is a modified form of Darcy's Law which governs the separation of melt from the matrix. The separation flux of liquid from solid $\phi(\boldsymbol{v}-\boldsymbol{V})$ is proportional to the permeability and flows down pressure gradients. Equation (4) is Stokes equation for creeping matrix flow and shows that the pressure gradients that make melt move depend both on the buoyancy difference between melt and solid and on the viscous deformation of the matrix. Equation (5) gives the permeability as a nonlinear scalar function of the pore spacing a, porosity and a dimensionless coefficient, b. Equation (5) is a convenient parametrization for a range of porosity/permeability relationships valid for small porosities ($\leqslant$ 10–20 %). More specific relations can be found in standard texts on porous flow (Dullien 1979; Scheidegger 1974; Bear 1988). The actual functional form of the permeability is not particularly crucial to the following discussion except for the important requirements that both the permeability, k_ϕ, and $\partial k_\phi/\partial\phi$ are increasing functions of porosity. Simple capillaric models for permeability suggest that a power law with $n\approx 2$–3 is a good approximation for natural systems. More detailed analysis of texturally equilibrated melt/solid networks gives similar results (Cheadle 1989; Von Bargen & Waff 1986).

Table 1. *Notation*

variable	meaning	value used	dimension
a	pore spacing (grain size)	10^{-3}–10^{-1}	m
b	constant in permeability	100–3000	none
$\mathscr{C}$	compaction rate (isotropic strain rate)	—	s^{-1}
g	acceleration due to gravity	9.81	m s^{-2}
k_ϕ	permeability	—	m^2
k_0	$= a^2\phi_0^n/b$ permeability at porosity ϕ_0	—	m^2
n	exponent in permeability	2–3	none
$\mathscr{P}$	$= P-\rho_f gz$ piezometric pressure	—	Pa
$\boldsymbol{q}$	$= \phi\boldsymbol{v}$ dimensionless melt flux	—	none
t	time	—	s
$\mathscr{U}^s$	matrix scalar potential	—	m^2 s^{-1}
$\boldsymbol{V}$	$= \nabla\times\boldsymbol{\Psi}^s+\nabla\mathscr{U}^s$ matrix velocity	—	m s^{-1}
$\boldsymbol{v}$	melt velocity	—	m s^{-1}
w_0	$= k_0\Delta\rho g/\phi_0\mu$ percolation velocity	—	m s^{-1}
x	horizontal cartesian coordinate	—	m
z	vertical cartesian coordinate	—	m
δ	$= \sqrt{(k_0(\zeta+\frac{4}{3}\eta)/\mu)}$ compaction length	100–10000	m
Γ	melting rate	—	kg m^{-3} s^{-1}
ζ	matrix bulk viscosity	10^{18}–10^{21}	Pa s
η	matrix shear viscosity	10^{18}–10^{21}	Pa s
ξ	$\eta/(\zeta+\frac{4}{3}\eta)$	$\frac{3}{7}$	none
ξ'	ξ/ϕ_0	—	none
μ	melt shear viscosity	1–10	Pa s
ρ_f	density of melt	2800	kg m^{-3}
ρ_s	density of matrix	3300	kg m^{-3}
$\Delta\rho$	$= \rho_s-\rho_f$	500	kg m^{-3}
ϕ	porosity	—	none
ϕ_0	reference porosity (constant)	0.005–0.04	none
ψ^s	matrix stream function (2D)	—	m^2 s^{-1}
$\boldsymbol{\Psi}^s$	matrix 3D vector potential	—	m^2 s^{-1}

(*b*) *Governing equations in potential form*: *constant viscosity, constant densities*

The governing equations (1)–(5) are similar to those for standard porous media flow with the important distinction that the matrix is able to deform viscously. For the problem of magma migration from the mantle, this behaviour must be allowed if these equations are to be consistent with mantle convection. It is the pressure gradients due to this additional viscous deformation that provide for most of the interesting new behaviour. For the case of constant matrix viscosities, (4) can be written

$$\nabla\mathscr{P} = -\eta\nabla\times\nabla\times\boldsymbol{V}+(\zeta+\tfrac{4}{3}\eta)\,\nabla\,(\nabla\cdot\boldsymbol{V})-(1-\phi)\,\Delta\rho g\boldsymbol{k} \tag{6}$$

to show that the pressure gradients due to viscous flow arise from two fundamentally different types of matrix deformation. The first term of (6) is the pressure gradient due to incompressible shear (rotational flow) of the viscous matrix. The second term is the gradient due to volume changes of the compressible matrix. The distinction between compressible and incompressible matrix deformation provides a convenient way to categorize the general behaviour of the governing equations. It should be stressed that 'compressible' matrix deformation refers to the ability of the matrix framework to expand and compact to produce changes in porosity in response to variations in the melt flux. The individual crystals that form this framework,

PHILOSOPHICAL TRANSACTIONS OF THE ROYAL SOCIETY A MATHEMATICAL, PHYSICAL & ENGINEERING SCIENCES

however, are incompressible. Incompressible flow refers to matrix shear without volume changes. By assuming constant viscosities, the pressure gradients due to the two basic modes of matrix deformation separate. Using Helmholtz's theorem, the matrix velocity field $\boldsymbol{V}$ can also be decomposed into incompressible and compressible flow fields:

$$\boldsymbol{V} = \nabla \times \boldsymbol{\Psi}^{\mathrm{s}} + \nabla \mathscr{U}^{\mathrm{s}}, \tag{7}$$

$\boldsymbol{\Psi}^{\mathrm{s}}$ is the vector potential governing rotational flows (in 2D $\boldsymbol{\Psi}^{\mathrm{s}}$ is the stream function). $\mathscr{U}^{\mathrm{s}}$ is a scalar potential governing irrotational flow. It is also useful to define the isotropic strain rate or 'compaction rate' as

$$\mathscr{C} = \nabla \cdot \boldsymbol{V}. \tag{8}$$

The compaction rate is simply the rate of volume change of the matrix. If $\mathscr{C} > 0$ the matrix is expanding; $\mathscr{C} < 0$ implies compaction. Given these definitions and letting ρ_{f}, and ρ_{s} be constant, (1)–(5) can be rewritten solely in terms of porosity and matrix deformation. Expanding (2) gives

$$\partial\phi/\partial t + (\nabla \times \boldsymbol{\Psi}^{\mathrm{s}} + \nabla \mathscr{U}^{\mathrm{s}}) \cdot \nabla\phi = (1-\phi)\,\mathscr{C} + \Gamma/\rho_{\mathrm{s}}. \tag{9}$$

Adding (1) and (2) and substituting (3) and (6) yields

$$-\nabla \cdot (k_\phi/\mu)\,(\zeta + \tfrac{4}{3}\eta)\,\nabla\mathscr{C} + \mathscr{C} = \nabla \cdot (k_\phi/\mu)\,[\eta \nabla \times \nabla^2 \boldsymbol{\Psi}^{\mathrm{s}} - (1-\phi)\,\Delta\rho g \boldsymbol{k}] + \Gamma\,\Delta\rho/\rho_{\mathrm{s}}\rho_{\mathrm{f}}. \tag{10}$$

Equations (7) and (8) imply

$$\nabla^2 \mathscr{U}^{\mathrm{s}} = \mathscr{C} \tag{11}$$

and taking the curl of (6) gives

$$\nabla^4 \boldsymbol{\Psi}^{\mathrm{s}} = -(\Delta\rho g/\eta)\,\nabla \times \phi \boldsymbol{k}. \tag{12}$$

Further details of the derivation, non-dimensionalization and a discussion of boundary conditions can be found in Spiegelman (1993*a*).

Equations (9)–(12) form a coupled system of hyperbolic, elliptic and bi-harmonic equations that can be solved by using standard techniques. While writing the equations in potential form may appear to obscure the physics, this decomposition actually makes the behaviour of viscous two-phase flow clearer by making the equations for incompressible and compressible matrix deformation explicit. This decomposition also allows these two modes to be solved for sequentially.

Equation (12) governs incompressible matrix deformation and is the Stokes equation for the creeping rotational flow of the matrix driven by horizontal porosity variations and boundary conditions. This equation is identical to that found in thermal convection. Here, however, the matrix convection is driven by variations in the amount of melt present rather than by variations in temperature. Considerable work has been carried out on incompressible two-phase shear flow, particularly at mid-ocean ridges (Rabinowicz *et al.* 1984; Spiegelman & McKenzie 1987; Phipps Morgan 1987; Ribe & Smooke 1987; Ribe 1988; Scott 1988; Scott & Stevenson 1989; Buck & Su 1989; Daly & Richter 1989; Cordery & Phipps Morgan 1992). Section 3*a* summarizes this work, and discusses its role in focusing melt movement beneath mid-ocean ridges.

Equations (9)–(11) govern compressible matrix deformation and have been less extensively studied. These equations can be combined to form a nonlinear dispersive wave equation for the evolution of porosity in space and time. The existence of nonlinear solitary wave solutions for porosity were demonstrated almost as soon as

the equations were derived (Scott & Stevenson 1984; Scott *et al.* 1986; Richter & McKenzie 1984; Barcilon & Richter 1986). These waves have been shown to exist in one, two and three dimensions and their stability has been discussed by Scott & Stevenson (1986) and by Barcilon & Lovera (1989). While this previous work shows that solitary waves are easily produced, their overall significance has not been well understood. The more general physics of compressible matrix deformation is presented in Spiegelman (1993*a*, *b*) which shows that these solitary waves are an essential feature of the governing equations and will form spontaneously from any perturbation in the melt flux. This work also investigates the effects of melting and freezing on the solitary waves and shows that many geologically reasonable initial conditions should develop solitary waves. The following section briefly reviews the behaviour of compressible flow that is important for understanding the behaviour of high permeability melt channels at ridges (§3*b*).

(*c*) *General behaviour of compressible flow*

The important behaviour of compressible matrix deformation is contained in (9) and (10). Equation (9) governs conservation of porosity and states that changes in ϕ are caused by matrix advection and the balance between volume changes of the matrix and melting. Equation (10) governs volume changes of the matrix and states that the compaction rate $\mathscr{C}$ depends on the divergence of the melt separation flux $\phi(\boldsymbol{v}-\boldsymbol{V})$ and the volume change on melting, i.e.

$$\mathscr{C} = -\nabla\cdot\phi(\boldsymbol{v}-\boldsymbol{V})+\Gamma\Delta\rho/\rho_{\mathrm{s}}\rho_{\mathrm{f}}. \tag{13}$$

Equation (10), however, has been rearranged to stress that it is an elliptic equation for the compaction rate. The right side of (10) contains volume changes due to spatial variations in the 'forced flux' and to volume changes on mass transfer. The forced flux contains the components of the melt separation flux driven by incompressible shear and by buoyancy. The left side of (10) shows that these forcing terms change the volume of the matrix (second term) and develop an opposing 'compaction flux'. The compaction flux arises from pressure gradients induced by the viscous resistance of the matrix to changing volume.

The first term (10) is perhaps the most important term in the governing equations. Dimensional analysis shows that pressure gradients due to volume changes of the viscous matrix only become significant when the melt flux varies over the compaction length

$$\delta = [k_\phi(\zeta+\tfrac{4}{3}\eta)/\mu]^{\frac{1}{2}}. \tag{14}$$

In many geological problems, δ is small (order 100–1000 m) and several authors (Ribe 1985; Ribe & Smooke 1987; Scott & Stevenson 1989) have proposed that the first term in (10) can be neglected for most geological problems. Other workers (Buck & Su 1989; Sotin & Parmentier 1989) have simply neglected this term altogether. The zero compaction length approximation reduces a potentially singular second order equation to a zero-order equation. In particular, Spiegelman (1993*a*) shows that the zero compaction length approximation reduces the equations for compressible flow to a single nonlinear wave equation that predicts porosity 'shock waves', travelling discontinuities in the porosity. Such shocks will result from any initial condition where the melt flux locally exceeds what can be readily extracted, for example, the injection of magma into a region of low permeability or a local increase in the melting rate. The shaded curves in figure 1 show the evolution of a simple initial condition

PHILOSOPHICAL TRANSACTIONS OF THE ROYAL SOCIETY A MATHEMATICAL, PHYSICAL & ENGINEERING SCIENCES

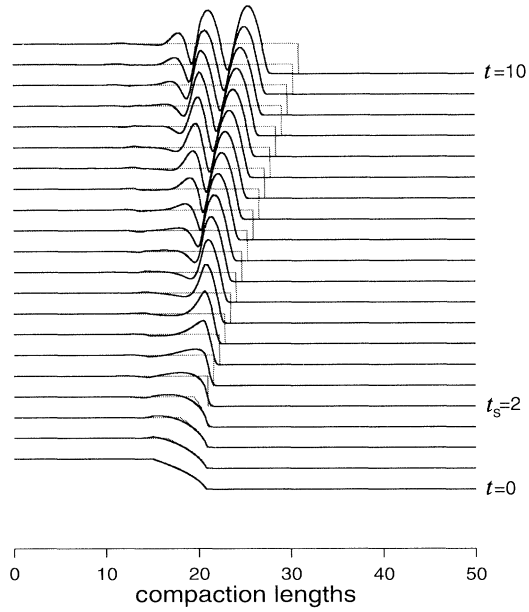

Figure 1. A comparison of approximate and full solutions for the evolution of porosity from an initial condition that develops into a perfect step function shock at time $t_s = 2$ in the zero compaction length approximation. The shaded lines show the analytic shock solution to the approximate equations. After $t = t_s$, this shock travels as a perfect step with $\phi_{max} = 1$, $\phi_1 = 0.2$ at constant velocity $c_s = 1.24$. The solid lines show the numerical solution to the full equations for the same initial condition. Until $t = t_s$ the full and approximate solutions are comparable. For $t \geqslant t_s$, viscous resistance of the matrix to volume changes causes the shock to disperse into a series of porosity maxima and minima. In this example, the leading porosity wave travels slower than the shock ($c \approx 0.8$) and each new wave forms further back relative to the matrix.

that forms a travelling step-function shock when the viscous resistance of the matrix is neglected. In the vicinity of the shock, however, viscous resistance to volume changes cannot be negligible and the approximation is not uniformally valid. The solid curves in figure 1 show the evolution of the identical initial condition using the full equations and shows that viscous resistance to volume changes causes the shock to disperse into a growing train of solitary waves. Figure 2 shows the long term evolution of porosity for a set of initial conditions that would produce simple shocks in the zero compaction length approximation. This figure shows that the amplitude of the solitary waves correlates with the size of the obstruction in flux (large steps produce large solitary waves) and that the dispersive wave trains can grow to span many compaction lengths and even allow for information to propagate backwards relative to the matrix (see figure 2 for $\phi_1 = 0.2$). Spiegelman (1993*b*) discusses and quantifies this dispersion and shows it to be consistent with the form of the governing equations. This work also shows that solitary waves are waves of volume fraction (porosity) and move faster than does the melt itself.

The solutions shown in figures 1 and 2 demonstrate the important processes that govern the separation of melt from solid. In general, porosity waves are a fundamental feature of these equations. These waves propagate because variations in the melt flux force the matrix to change volume. As long as the flux is an increasing function of porosity and the matrix is deformable, then porosity waves will exist. The actual speed and behaviour of the porosity waves, however, depends on the

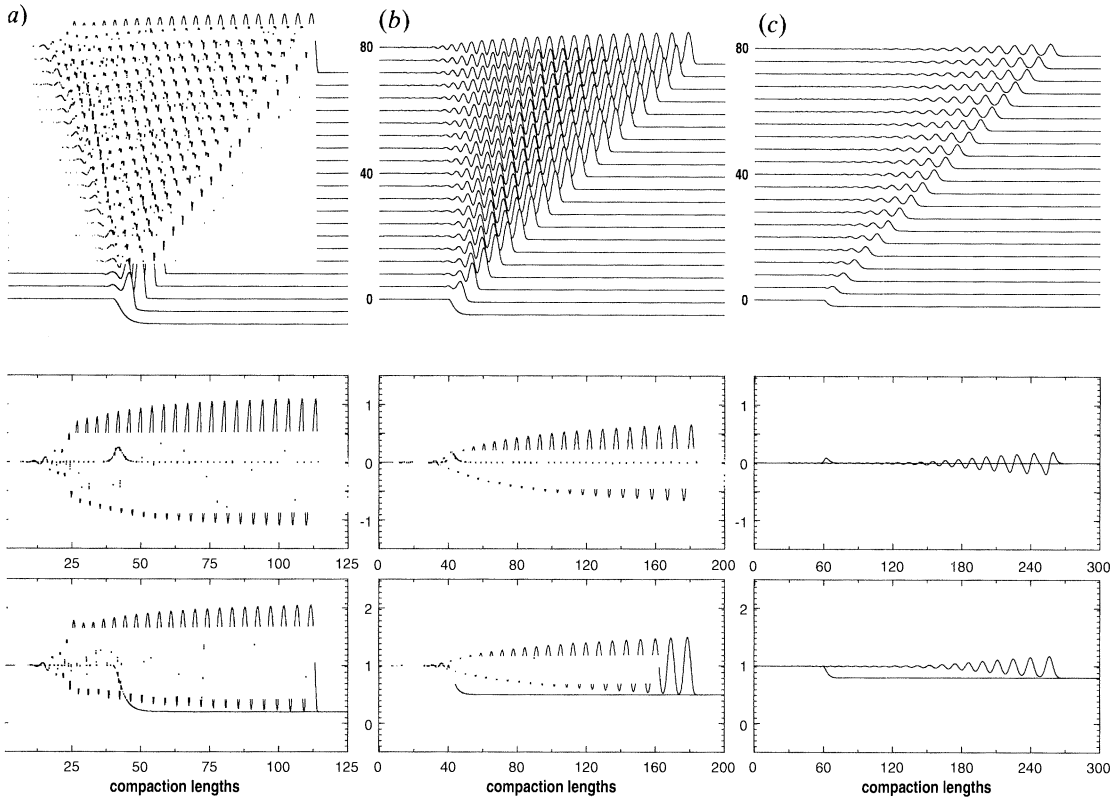

Figure 2. The long-term evolution of an initial condition similar to that in figure 1 showing the relationship between the amplitude of solitary waves and the size of the initial obstruction. In the absence of viscous dispersion, this initial condition would evolve to a travelling step function shock with $\phi_{\max} = 1$, $\phi_{\min} = \phi_1$. Viscous resistance to volume changes causes all shocks to disperse into rank-ordered dispersive wave trains of solitary waves. For each value of ϕ_1, the top figure shows porosity profiles against time ($t = 0$–80). Bottom two figures superpose initial ($t = 0$) and final ($t = 80$) profiles for compaction rate and porosity. All grids have $4\phi_1^{-\frac{3}{2}}$ grid points/compaction length for accurate resolution (Spiegelman 1993*b*). (*a*) A large-amplitude change in porosity ($\phi_1 = 0.2$) develops into a large-amplitude, slow moving, back-propagating wave train. (*b*) A smaller obstruction ($\phi_1 = 0.5$) develops a smaller-amplitude, faster wave train (note the difference in scales) with all new waves initiating at *ca.* $z = 40$. (*c*) The smallest obstruction ($\phi_1 = 0.8$) produces a small-amplitude, fast moving, forward propagating, wave train.

relationship between permeability and porosity. For most commonly used permeability–porosity relationships, $\partial k_\phi/\partial\phi$ is an increasing function of porosity; therefore, regions of high porosity (high melt flux) will propagate faster than regions of lower porosity and can cause the porosity gradients to steepen. If there was no viscous resistance of the matrix to changing volume, this steepening would continue until shocks form. However, in the vicinity of a rapid change in flux, viscous resistance cannot be negligible and in general it will cause the porosity to disperse into nonlinear solitary waves.

It should be stressed that because porosity gradients can steepen, viscous effects can become important even for smooth initial conditions where compaction effects are initially negligible. Spiegelman (1993*a*) presents the general criteria for shock formation using the zero compaction length approximation. Figures 1 and 2 also

PHILOSOPHICAL TRANSACTIONS OF THE ROYAL SOCIETY A MATHEMATICAL, PHYSICAL & ENGINEERING SCIENCES

show that, once viscous effects become important, the obstruction in flux does not remain localized, but rather, excites the growth of additional solitary waves. Because of this dispersion, even initially localized disturbances in the melt flux can eventually affect the entire partly molten region. Thus a small compaction length does not imply a negligible compaction term. If these equations are an accurate description of magma migration in the mantle, the clear implication is that the episodicity of magmatism may reflect the basic processes of migration from the source region.

3. Using the theory: applications to mid-ocean ridges

The simple model problems of the previous section demonstrate the important behaviour of compressible matrix deformation, but do so in a somewhat abstract manner. The purpose of the following section is to develop a better understanding of the behaviour of the governing equations in a more geological context. Here we will use the theory of viscous two-phase flows to consider some of the processes that may be occurring at mid-ocean ridge spreading centres. In particular, this section is motivated by the important observation of the extreme narrowness of the neo-volcanic zone. As many authors have noted (MacDonald 1982; Detrick *et al.* 1987; Burnett *et al.* 1989; Toomey *et al.* 1990; Caress *et al.* 1992) a variety of geophysical data strongly suggest that the entire 6 km thickness of oceanic crust is emplaced within approximately 2 km of the ridge axis. The implications of this observation are clear. Either the melting region at depth is of a comparable width, or there must be some mechanism for lateral migration of melt to the ridge axis. The following sections will demonstrate three different mechanisms that can produce focused volcanism. The first two mechanisms depend on incompressible matrix shear. The third mechanism relies upon the behaviour of compressible matrix deformation. The three mechanisms illustrate the broad range of behaviour inherent in the equations for flow in deformable porous media and suggest that both incompressible and compressible matrix deformation may be significant in magma migration.

(a) *Incompressible flow: focusing by mantle shear*

The first two mechanisms for focused ridge volcanism rely on the ability of the matrix to shear. At mid-ocean ridges there are always two primary sources of mantle shear. The first is shear driven by boundary conditions, in this instance the spreading plates. The second is mantle shear driven by internal buoyancy variations. By rescaling (12) using the scaling relations in table 2, the dimensionless 2D equations for incompressible porosity driven convection can be written

$$\nabla^4 \psi^s = R\, \partial\phi/\partial x, \tag{15}$$

where $R = \phi_0 \Delta\rho g d^2/\eta U_0$ is the single parameter which measures the relative contributions of buoyancy driven shear to plate driven shear. Here d is the depth of the partly molten layer (*ca.* 50–60 km), U_0 is the half-spreading rate, and ψ^s is the 2D matrix stream function. Comparison with the dimensionless equations for thermal convection

$$\partial T/\partial t + (\nabla \times \psi^s \boldsymbol{j}) \cdot \nabla T = \nabla^2 T, \tag{16}$$

$$\nabla^4 \psi^s = Ra\, \partial T/\partial x \tag{17}$$

shows that R plays exactly the same role as the Rayleigh number in thermal convection and measures the relative contributions of buoyancy forces to viscous plate driving forces. When R is large, buoyancy dominates and vigorous convection

Table 2. *Scaling relations for porosity driven convection*
(Primes denote dimensionless variables.)

variable	scale parameter	scaling relation
porosity	maximum porosity	$\phi = \phi_0 \phi'$
distance	melting depth	$(x, z) = d(x', z')$
		$\nabla = \nabla'/d$
velocity	plate velocity	$(\boldsymbol{v}, \boldsymbol{V}) = U_0(\boldsymbol{v}', \boldsymbol{V}')$
stream function		$\psi^s = dU_0 \psi^{s'}$

can occur. Unlike thermal convection however, it is horizontal variations in porosity, rather than temperature, that drive convection. Moreover, porosity is governed by a dispersive wave equation, while temperature is diffusive. When R is small, convection is negligible and mantle flow is dominated by the boundary conditions.

Figure 3*a* and *b* show the full steady-state solutions for the porosity, solid flow and melt flow for two end-member solutions in a geometry appropriate for ridges. These solutions are actually the end result of a long time dependent calculation that relaxes to steady state due to the free flux boundary condition at the top of the box. The possible time dependent effects of a freezing lid are discussed in §3*b*. In this solution, the dimensional melting rate is given by

$$\Gamma = \begin{cases} \rho_s F_{\max} W/d & W > 0, \\ 0 & W < 0 \quad \text{and on closed streamlines,} \end{cases} \tag{18}$$

which approximates melting by adiabatic decompression. $F_{\max}$ is the maximum degree of melting experienced on axis (here $F_{\max} = 0.25$), W is the vertical component of the matrix velocity and d is the depth of the melting region. Equation (18) states that any piece of fertile mantle melts at a rate proportional to the upwelling velocity, while material that moves sideways or down or along a closed flow line does not melt. Figure 3*c*, *d* shows the melting rate fields for these solutions.

When R is small (figure 3*a*) the matrix flow is essentially corner flow which can develop large non-hydrostatic pressure gradients that focus the flow of melt. The physics of melt focusing is discussed in detail in Spiegelman & McKenzie (1987) (see also Phipps Morgan 1987; Ribe 1988), who use an analytic constant porosity corner flow solution without melting. When melting is added, the porosity field is no longer constant, nevertheless, the basic behaviour of melt flow remains the same. As noted by earlier authors, this melt focusing provides a simple mechanism for extracting melt from a wide region at depth and extruding it at the surface in a narrow region. The principal geological problem with this solution, however, is that the actual melting region due to corner flow is quite wide and usually wider than the extraction zone, thus not all of the melt is extracted. Moreover, for reasonable estimates of melting depth and spreading rates, the viscosities required are large (i.e. 10^{20}–10^{21} Pa s). Such values have been considered 'unreasonable' although the rheology of two-phase melt-solid assemblages is still only poorly understood (Cooper & Kohlstedt 1984; Cooper & Kohlstedt 1986; Borch & Green 1990).

When viscosities are lower (more precisely for large values of R) then the focusing effect becomes negligible and internal sources of buoyancy become important. When the principal source of buoyancy in the melting region is due to lateral variations in melt content (Rabinowicz *et al.* 1984; Scott & Stevenson 1989; Buck & Su 1989) the effect is to produce an additional convective roll superposed on the plate driven

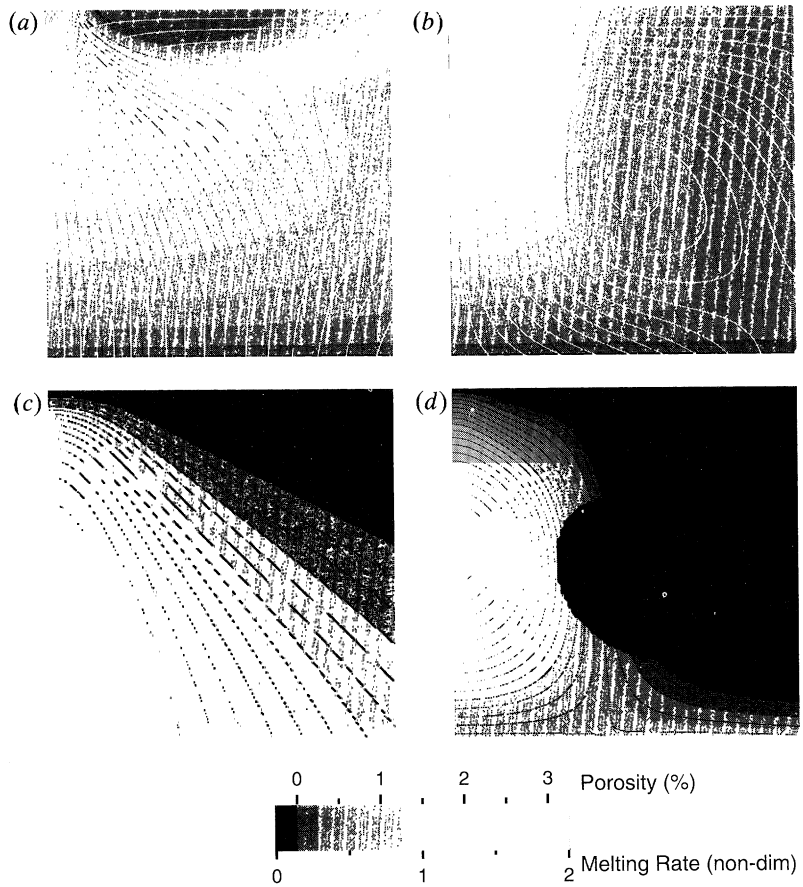

Figure 3. 2D solutions for the flow of melt and solid for a simple ridge spreading geometry demonstrating the effects of passive against active mantle flow. The top two parts show porosity, melt flow (black curves) and matrix flow (white curves). The bottom two figures show the dimensionless melting rate which is proportional to upwelling rate for 'fertile' upwelling mantle. $\Gamma = 0$ on closed streamlines or downwelling regions. Each part shows the right half of the melting region. The vertical scale is the melting depth (50–60 km) and there is no vertical exaggeration. R is related to the Raleigh number and measures the relative contribution of buoyancy forces to viscous forces. (*a*) Plate-dominated flow, $R = 0.0357$. When shear is dominated by boundary conditions, the forced shear of the viscous matrix can produce large pressure gradients that focus the flow of melt. (*b*) Buoyancy driven flow, $R = 56.28$. For lower viscosities or plate velocities, variations in melt content can drive additional small-scale convection which narrows the width of the upwelling region. (*c*) Melting rate field for plate driven shear, (*d*) and for buoyancy driven shear.

corner flow solution (figure 3*b*). This additional convection produces a narrow, fast upwelling zone beneath the ridge axis which narrows the region of melting. However, to produce a melting region with a width comparable to the neo-volcanic zone requires very large values of R which in turn requires very small matrix viscosities (Buck & Su 1989). For values of viscosity that are considered reasonable (10^{18}–10^{19} Pa s), the melting region is still approximately 20 km wide (figure 3*b*) and there is no additional melt focusing due to forced matrix shear. When the buoyancy is driven solely by depletion effects or temperature differences (Sotin & Parmentier 1989; Parmentier & Phipps Morgan 1990; Sparks & Parmentier 1990*b*, *a*; Cordery & Phipps Morgan 1992) the narrowing is much more subdued.

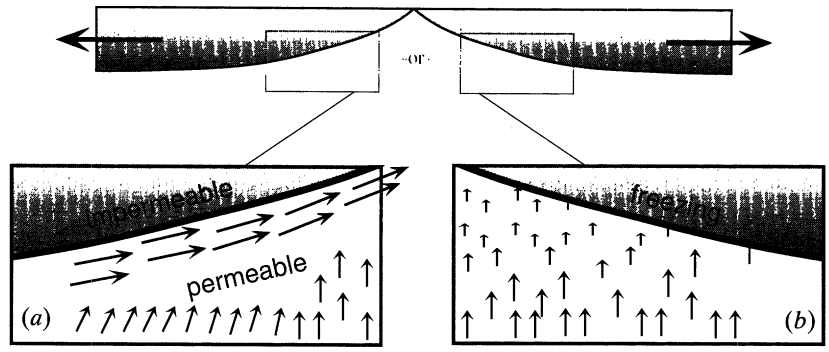

Figure 4. The two fundamental effects of freezing on the flow of melt near the top of the partly molten region. (*a*) Melt channelling: because the cooling plates form a natural sloping impermeable barrier to melt flow, channels may arise that transport melt to the ridge axis. (*b*) Simple freezing: as melt approaches the freezing boundary, it will be converted to solid which is transported away by the spreading plates.

The point of figure 3 is that both 'passive' and 'active' flow models are really end-member solutions of exactly the same equations. Both rely on the ability of the matrix to shear, the only difference between these two solutions is which of the two sources of shear dominate. If plate driving forces are sufficiently large, melt focusing may be sufficient to produce the narrow neo-volcanic zone. Alternatively, if the buoyancy forces are significant, then narrowed upwelling may play a part. It is not possible, however, to have both effects simultaneously, and neither process, by itself, appears to be sufficient for geologically reasonable values of R. Both processes, however, may be assisted by an additional mechanism for focusing that relies on compressible matrix deformation.

(*b*) *Compressible flow: freezing induced melt channels*

The principal result of §2*c* is that obstructions in the melt flux will shed solitary waves. At mid-ocean ridges one of the principal obstructions to the flow of melt is the presence of a frozen, impermeable lid produced by the spreading and cooling plates. This section will show that the solitary waves that develop due to freezing can form channels that guide the melt to the ridge axis.

One of the oldest suggestions for the lateral flow of melt at ridges is that melt percolates under gravity until it encounters the impermeable lid, develops some form of melt channel along the base of the sloping impermeable region and flows to the ridge axis. Figure 4*a* shows this channelling behaviour schematically. More recently, Sparks & Parmentier (1991) have begun to quantify this process and use results from a series of steady state 1D melt segregation problems to suggest that such a high porosity channel should exist. While this mechanism is appealing, the actual nature of the impermeable boundary is somewhat problematic. The principal problem is that the reason this boundary is impermeable is that it is simply too cold to allow the presence of any partial melt (i.e. it is a freezing boundary). Therefore, an equally plausible solution is that, as the melt approaches this boundary, it is converted to solid and is carried off by the spreading plates (figure 4*b*). It is not obvious which of these two effects of freezing actually controls the flow of melt near the top of the partly molten zone.

Rather than attempting to solve the full flow of melt and solid and its attendant temperature field beneath a ridge, figure 4 suggests that it may be sufficient to

PHILOSOPHICAL TRANSACTIONS OF THE ROYAL SOCIETY A MATHEMATICAL, PHYSICAL & ENGINEERING SCIENCES

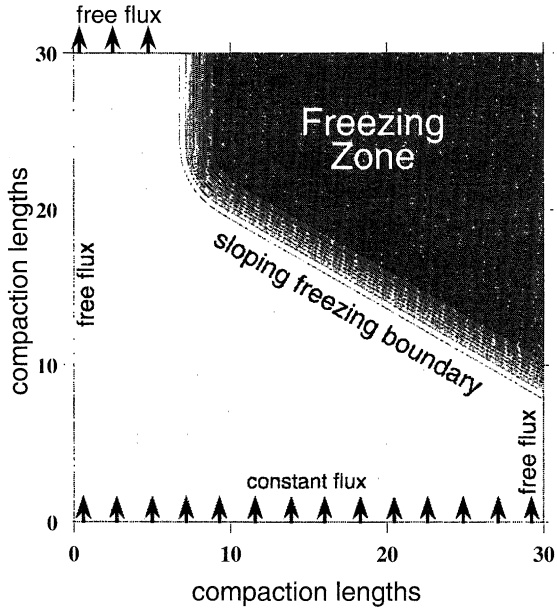

Figure 5. Geometry and boundary conditions used to investigate melt migration near a sloping freezing boundary. Freezing occurs in the darker region marked freezing zone. Contours and shading show values of the imposed freezing rate field $\Gamma(\boldsymbol{x})$. The freezing length, $\delta_f = 1/\Gamma_0$ is approximately the length scale (in compaction lengths) over which a uniform melt flux would freeze completely. There is no matrix shear. Boundary conditions are constant melt flux into the base, free flux out the top and sides. The problem is non-dimensional with length scaled to the compaction length δ, porosity scaled to the uniform background porosity ϕ_0, and velocities to the background melt velocity w_0. Typical values for δ are 100–1000 m, for ϕ_0 are 1–10 % and for w_0 are 0.1–1 m a^{-1}.

understand the 2D flow of melt near a sloping freezing boundary. To that end, I have constructed a simple model problem which shows that both effects of freezing are actually possible and that again there is a single parameter that controls whether channels form.

Figure 5 illustrates the geometry and boundary conditions of the model. It consists of a two-dimensional region, 30 compaction lengths on a side. The freezing rate is imposed using the function

$$\Gamma = \tfrac{1}{4}\Gamma_0[1-\tanh(\boldsymbol{k}\cdot\boldsymbol{x})][1+\tanh(k_1(x-x_1))], \tag{19}$$

where Γ_0 is the maximum freezing rate in the interior of the freezing zone and $\boldsymbol{k}$ is a vector that is normal to the sloping boundary. The final hyperbolic tangent term is used to smoothly truncate the sloping freezing front at a distance x_1 from the left edge of the box. This truncation is used to avoid the interaction of the freezing zone with the boundaries of the region. While (19) appears somewhat complicated, the geometry is actually straight-forward and contours of Γ are shown in figure 5. For simplicity, this problem neglects any matrix shear deformation although, beneath a ridge, it is the large scale matrix flow that governs the thermal structure, and therefore the shape of the freezing region. Nevertheless, as long as the melt velocity is much greater than the matrix velocity, then the approximation of a fixed freezing region with no matrix shear is valid. Further experiments consider the effects of small amounts of matrix flow but do not change the basic results shown here.

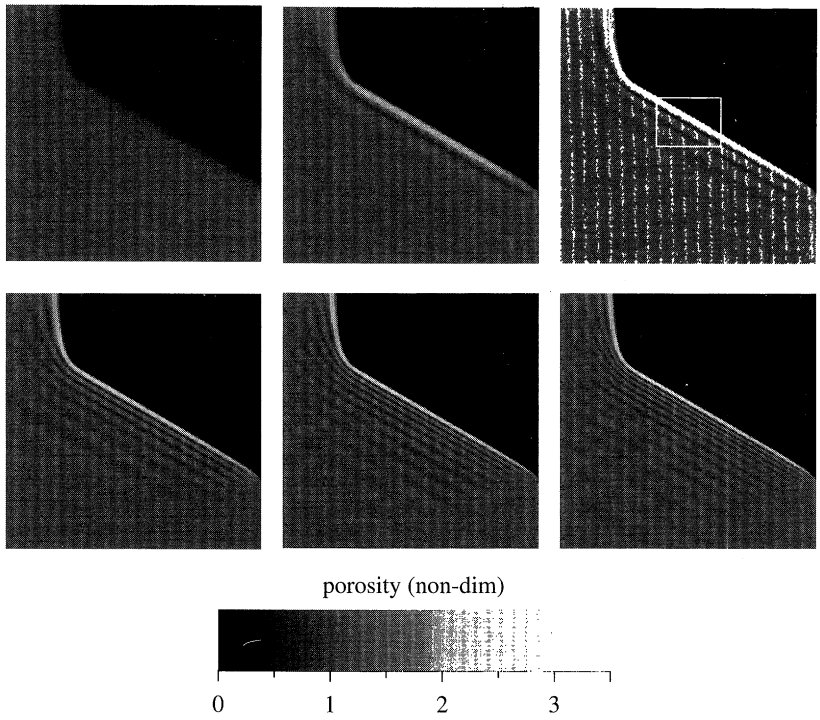

Figure 6. Evolution of porosity near a freezing zone with a rapid freezing rate ($\Gamma_0 = -2.0$) showing the development of high permeability melt channels near the freezing boundary. Each box is 30×30 compaction lengths on a side and shading shows porosity relative to the background porosity ($\phi = 1$) for dimensionless times $t = 0$, 10, 20 (top row), 40, 60, 80 (bottom row). A dimensionless time of 30 is the time required for a completely incompatible trace element to travel across the box at the background melt velocity. The initial condition is the steady-state solution given by the zero compaction length approximation where the melt can only percolate vertically and then freeze. At $t = 10$ the excess melt that cannot be accommodated by freezing begins to accumulate at the boundary in a growing channel ($\phi_{\max} \approx 2.4$). With time the initial channel grows to a porosity approximately 3.5 times greater than the background. Rather than growing into a single channel, however, the growth of each channel initiates the formation of a new channel below it in the same manner as the dispersion of solitary waves. The white box at $t = 20$ is the region depicted in figure 7*a*.

Boundary conditions on the melt flux are a constant flux in to the bottom of the box, and the melt flux out of the top, right and left boundaries is free to adjust during the calculation. Detailed descriptions of numerical techniques and boundary conditions are given in Spiegelman (1993*a*, *b*). The initial condition for each run was the steady-state solution predicted by the zero compaction length approximation. In this approximation, the melt flux is driven solely by gravity and is exactly balanced by the freezing rate. Thus the initial condition for the porosity is given implicitly by the dimensionless flux balance

$$k_\phi(1-\phi_0\,\phi)-(1-\phi_0) = \int_0^z \frac{\rho_f\,\Gamma(x,z)}{\rho_s}\,\mathrm{d}z \tag{20}$$

for $\phi \geqslant 0$. Any variation from this initial condition during a calculation results from the term governing viscous resistance of the matrix to volume changes. This initial condition produces a freezing region of approximate 'freezing width' $\delta_f = 1/\Gamma_0$ over

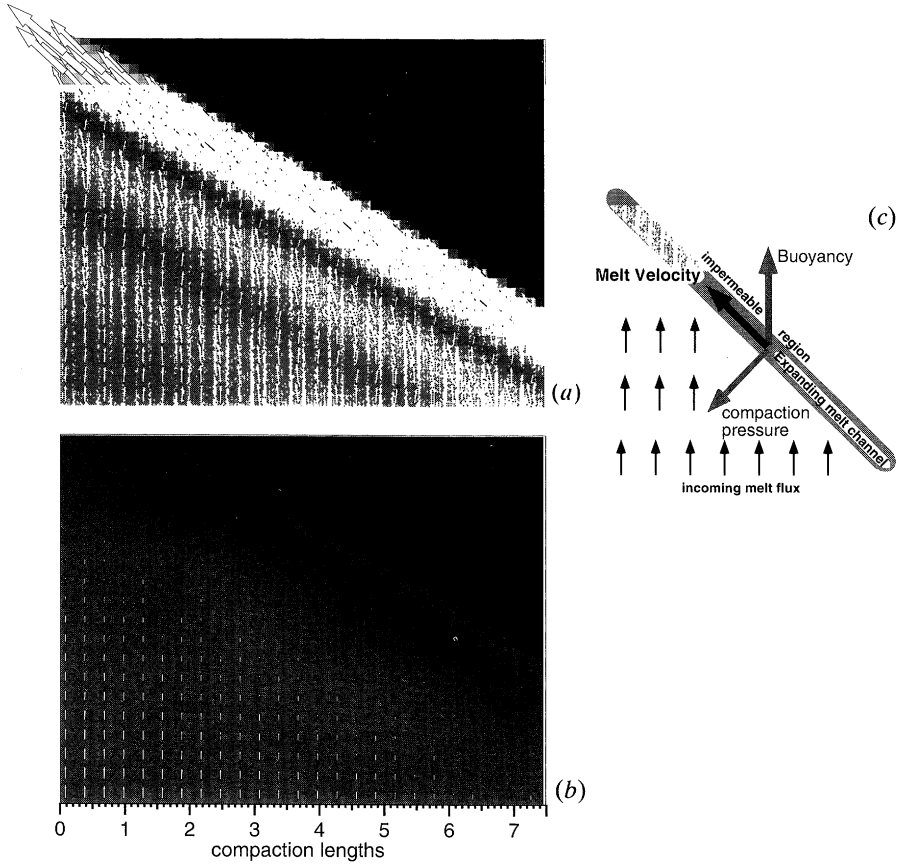

Figure 7. Close-up of the freezing boundary at $t = 20$ showing melt flux vectors for rapid and slow freezing rates. (*a*), (*b*) The 7.5×5.7 compaction length regions marked in figures 6 and 8. (*a*) Rapid freezing rate ($\Gamma_0 = -2.$): This figure shows that not only does the obstruction in flux cause porosity to increase near the freezing boundary, but also that the melt in these channels travels laterally. (*b*) When the freezing rate is slower ($\Gamma_0 = -0.1$), melt only percolates vertically. (*c*) Schematic diagram showing pressure gradients that make the melt flow laterally. When the melt flux is reduced by freezing over many compaction lengths, the compaction pressure is negligible and no channels form.

which the porosity decreases from the background porosity to impermeability. Note that the larger the freezing rate, the narrower the width of the freezing region. We now show that the larger the freezing rate, the more likely high permeability melt channels are to form.

(i) *Results*

Figure 6 shows the evolution of porosity for a rapid freezing rate and shows how the channels grow. When the freezing rate is large, the transition from the high permeability background to impermeability occurs over a distance comparable to the compaction length (here the width of the freezing layer is *ca.* 2δ) and the upwelling melt can 'see' the obstruction caused by the rapid change in permeability. Locally, the influx of melt is greater than can be consumed by freezing and the deformable matrix expands to accommodate the excess flux. This expansion leads initially to the growth of a high porosity channel near the freezing boundary ($t = 20$). Because the

PHILOSOPHICAL TRANSACTIONS OF THE ROYAL SOCIETY A MATHEMATICAL, PHYSICAL & ENGINEERING SCIENCES

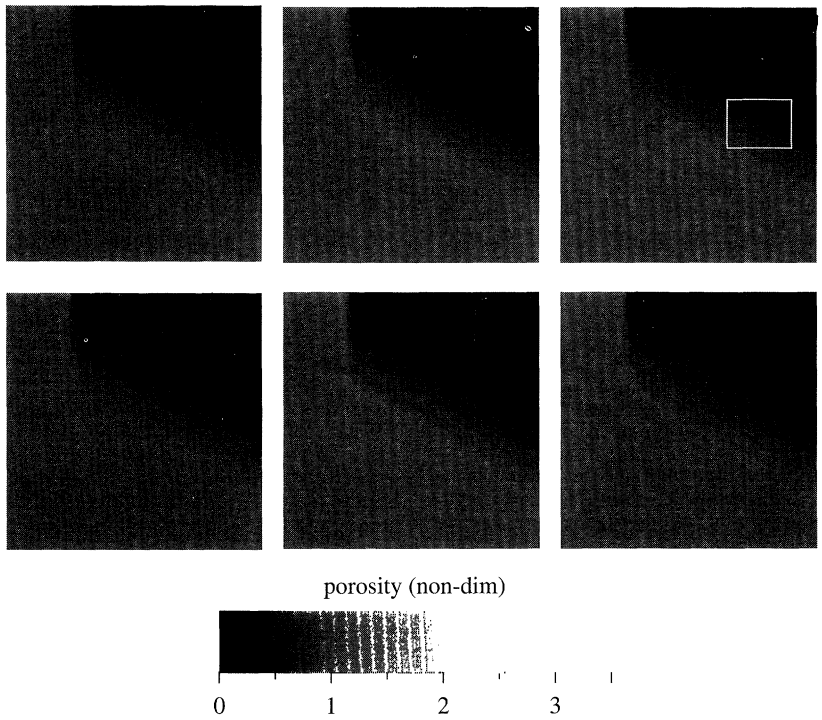

Figure 8. Evolution of porosity near a freezing zone with a slow freezing rate $\Gamma_0 = -0.1$ ($t = 0$, 10, 20 (top row), 40, 60, 80 (bottom row). When freezing occurs over a region that is large compared to the compaction length, viscous pressure gradients are negligible and only weak channels form. With time, this solution develops a weak oscillation that is related to the dispersion of solitary waves (§2*c*), however, as a first approximation, this solution maintains steady state. The white box at $t = 20$ is the region depicted in figure 7*b*.

matrix is viscous, however, these volume changes generate additional pressure gradients that deflect the flow of melt away from the vertical and along the boundary. Figure 7*a* shows a close-up of melt flow in the channel at $t = 20$. In this problem, the dimensional melt flux is approximately

$$\phi \boldsymbol{v} = -k_\phi[(\zeta + \tfrac{4}{3}\eta)\nabla\mathscr{C} - \Delta\rho g \boldsymbol{k}]. \tag{21}$$

The term $(\zeta + \frac{4}{3}\eta)\mathscr{C}$ is the 'compaction pressure', the pressure induced by volume changes of the viscous matrix. The melt is driven vertically by buoyancy and away from the expanding channel by gradients of the compaction pressure which is always normal to the interface (see figure 7*c*). The net melt flux is therefore at an angle to the vertical. These compaction pressure gradients, however, only become significant when the melt flux varies over the compaction length. When freezing is distributed over many compaction lengths (figures 7*b*, 8), the compaction pressure is negligible. In this case, melt percolates vertically due to buoyancy alone and freezes into place without developing significant melt channels. Figure 8 shows the time evolution of porosity for gradual freezing and is steady state to a first approximation.

This problem shows that if the freezing zone is sufficiently narrow, high permeability melt channels can form to transport melt along the boundary. When channelling occurs, the flow is strongly time dependent. Rather than forming a single channel, a whole rank ordered set of channels forms, all oriented parallel to the

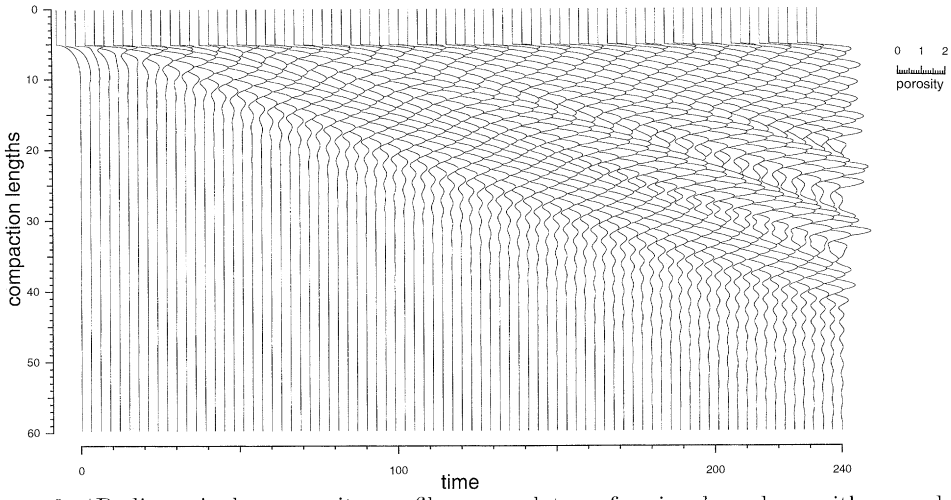

Figure 9. 1D dimensionless porosity profiles normal to a freezing boundary with a moderate freezing rate showing the development of a large dispersive train of melt channels. This calculation includes some flow of solid through the freezing region. The ratio of the solid velocity to the melt velocity is $W_0/w_0 = 0.01$, and freezing occurs over five compaction lengths from $z = 5$–10. The formation of these channels is similar to that for the dispersive solitary wave trains, however, these channels become absorbed in the freezing region. The channels form spontaneously without any time-dependent forcing. This problem appears to have no steady-state solution.

boundary. This behaviour is precisely the same phenomenon seen in the dispersion of solitary waves (§2*c*). In fact these channels are simply another manifestation of the solitary waves, however, they are pinned in place and take their overall form from the freezing boundary. Additional experiments suggest that, in addition to the two principally steady-state solutions shown here, there is also a strongly time-dependent régime where moderate amplitude channels can form but are transient. Figure 9 shows the detailed evolution of porosity taken in a 1D profile normal to the freezing boundary. The solution shown in figure 9 allows the matrix to advect porosity into the freezing region, which may affect the time dependence of the channels. In the time dependent régime, the initiation of channels can propagate far into the interior possibly producing an overall anisotropy in the large scale permeability that aligns itself with the freezing boundary. Lateral flow caused by any additional channels far from the freezing boundary, however, does not have to compete with freezing.

This simple model suggests that the existence or otherwise of channels in the Earth is controlled primarily by the ratio of the compaction length to the freezing length. Calculations based on the 1D steady-state thermal structure of an upwelling column (Sparks & Parmentier 1991; Spiegelman 1991) suggest that channelling may be an important mechanism for at least some lateral flow. However, more work needs to be done to consider the effects of channelling for larger-scale 2D and 3D problems. It should be stressed that this mechanism is completely different from the mechanisms that rely on incompressible shear (§3*a*) and can work in conjunction with both passive and active matrix flows. Compressible matrix deformation and the growth of channels are small-scale boundary layer phenomena that only depend on the local structure of the freezing zone. The structure of the freezing zone, however, depends on the large scale 2D and 3D flow and thermal structure of the mantle. This extreme variation in scales of processes is characteristic of the governing equations

PHILOSOPHICAL TRANSACTIONS OF THE ROYAL SOCIETY A MATHEMATICAL, PHYSICAL & ENGINEERING SCIENCES

and makes accurate resolution of both compressible and incompressible effects numerically difficult. Nevertheless, if the local parameters that control channelling can be derived for any given solution for large-scale mantle flow, it becomes straightforward to discover whether melt channels influence lateral melt migration.

4. Summary

The purpose of this paper is to illustrate and clarify the wide range of behaviour inherent in the equations governing flow in viscously deformable porous media. It should be stressed this behaviour arises because the matrix is permeable and can deform viscously. Provided that the melt is interconnected everywhere, these equations form a macroscopic description of magma migration and make no assumptions about the microscopic distribution of melt. Clearly, as the functional form of the permeability and rheology change, the quantitative solutions to the equations will also change.

It is the ability for the matrix to deform viscously that adds most of the interesting new behaviour to these equations. In particular, this paper demonstrates that the matrix can deform in two fundamentally different ways. Because the matrix can expand and compact, variations in melt flux can actually propagate through the matrix as porosity waves. These waves are an essential feature of the governing equations and will form spontaneously from any region where more melt is produced or injected than can be readily extracted. Compressible matrix deformation also controls the flow of melt around obstacles such as the impermeable top of the partly molten zone. From the simple solutions shown here, it is clear that the compaction length is the only intrinsic length scale governing compressible matrix deformation. While the compaction length can be quite small it cannot in general be neglected. Rather, these problems show that a small compaction length implies that viscous effects will become important in narrow boundary layers. However, because of the dispersive behaviour of these equations, initially localized boundary layers can propagate away from the region of initial disturbance. A surprising but potentially important result is that *information* about obstructions in the melt flux can propagate backwards while the melt can only propagate in a forward direction. Eventually the entire partly molten region can become affected. Because of this behaviour, it is possible to construct simple initial conditions that never relax to steady state (see figures 2 and 9).

The second mode of deformation is incompressible matrix shear which controls porosity driven convection. At ridges the vigour of convection is determined by the balance of shear driven by boundary conditions and internal buoyancy forces. While porosity driven convection is superficially similar to thermal convection, it should be stressed that porosity does not behave in the same manner as temperature. Therefore, the stability of two-phase regions to small perturbations may be quite different from that expected in thermal convection. It should also be noted that incompressible matrix deformation is sensitive to the largest length scales in the problem, namely the size of the partly molten region. However, compressible flow is sensitive to the smallest length scale. Because of this disparity in length scales, accurate large-scale numerical solutions for the flow of both melt and solid become computationally expensive. For this reason, most numerical solutions for incompressible two-phase flow either neglect viscous compaction effects or neglect the flow of melt altogether. Nevertheless, the interaction between incompressible and

PHILOSOPHICAL TRANSACTIONS OF THE ROYAL SOCIETY A MATHEMATICAL, PHYSICAL & ENGINEERING SCIENCES

compressible matrix deformation needs to be better understood. For example, large-scale solid flow controls the structure of the freezing boundary and therefore of the behaviour of the melt channels. Because the melt channels are dispersive, however, it is possible for compressible effects to grow to scales that might influence porosity driven convection. Because both incompressible and compressible mechanisms can contribute to melt focusing, it is important to understand the behaviour of the full set of equations.

Given the wide range of behaviour inherent in the governing equations, some of the geological implications of these results are clear. The melt extraction process should be inherently episodic in space and time. This episodicity should manifest itself in the volume, geometry and timing of eruptions. Given accurate forward solutions, it is straightforward to calculate the effects of geologically reasonable two-phase flows on geophysical and geochemical observables. For example, if we understood the coupling between melt content and seismic velocity, we could determine how well partly molten zones can be imaged. Present work is considering the effect of melt segregation on trace element chemistry and suggests that the spatial and temporal variations in chemistry may be a good indicator of the geodynamic process occurring at depth (Spiegelman 1992).

Many thanks to Dan McKenzie and Tim Elliot for useful discussions. This work was supported by NSF Grants OCE90-12572 and OCE91-14959 and is Lamont-Doherty Geological Observatory Contribution no. 4959.

References

Barcilon, V. & Lovera, O. 1989 Solitary waves in magma dynamics. *J. Fluid. Mech.* **204**, 121–133.

Barcilon, V. & Richter, F. M. 1986 Non-linear waves in compacting media. *J. Fluid Mech.* **164**, 429–448.

Bear, J. 1988 *Dynamics of fluids in porous media*. New York: Dover.

Borch, R. S. & Green, H. W. 1990 Experimental investigation of the rheology and structure of partially molten lherzolite deformed under upper mantle pressures and temperatures. *Eos, Wash.* **71**, 629.

Buck, W. R. & Su, W. 1989 Focused mantle upwelling below mid-ocean ridges due to feedback between viscosity and melting. *Geophys. Res. Lett.* **16**, 641–644.

Burnett, M., Caress, D. & Orcutt, J. 1989 Tomographic image of the magma chamber at 12° 50′ N on the East Pacific Rise. *Nature, Lond.* **339**, 206–208.

Caress, D. W., Burnett, M. S. & Orcutt, J. A. 1992 Tomographic image of the axial low velocity zone at 12° 50′ N on the East Pacific Rise. *J. geophys. Res.* **97** (B6), 9243–9264.

Cheadle, M. 1989 Properties of texturally equilibrated two-phase aggregates. Ph.D., University of Cambridge.

Cooper, R. & Kohlstedt, D. 1984 Solution-precipitation enhanced diffusional creep of partially molten olivine-basalt aggregates during hot pressing. *Tectonophys.* **107**, 207–233.

Cooper, R. & Kohlstedt, D. 1986 Rheology and structure of olivine-basalt partial melts. *J. geophys. Res.* **91**, 9315–9323.

Cordery, M. & Phipps Morgan, J. 1992 Melting and mantle flow beneath a mid-ocean spreading center. *Earth planet. Sci. Lett.* **111**, 493–516.

Daly, S. F. & Richter, F. M. 1989 Dynamical instabilities of partially molten zones: solitary waves vs. Rayleigh Taylor plumes. *Eos, Wash.* **70**, 499.

Detrick, R., Buhl, P., Vera, E., Mutter, J., Orcutt, J., Madsen, J. & Brocher, T. 1987 Multi-channel seismic imaging of a crustal magma chamber along the East Pacific Rise. *Nature, Lond.* **326**, 35–41.

Drew, D. 1971 Average field equations for two-phase media. *Stud. appl. Math.* **50**, 133–166.

Drew, D. 1983 Mathematical modeling of two-phase flow. *An. Rev. Fluid Mech.* **15**, 261–291.

Dullien, F. 1979 *Porous media fluid transport and pore structure*. New York: Academic Press.

Fowler, A. 1985 A mathematical model of magma transport in the asthenospere. *Geophys. Astrophys. Fluid Dyn.* **33**, 63–96.

MacDonald, K. 1982 Mid-ocean ridges: fine scale tectonic, volcanic, and hydrothermal processes within the plate boundary zone. *A. Rev. Earth planet. Sci.* **10**, 155–190.

McKenzie, D. 1984 The generation and compaction of partially molten rock. *J. Petrol.* **25**, 713–765.

Parmentier, E. M. & Phipps Morgan, J. 1990 The spreading rate dependence of three-dimensional spreading center structure. *Nature, Lond.* **348**, 325–328.

Phipps Morgan, J. 1987 Melt migration beneath mid-ocean spreading centers. *Geophys. Res. Lett.* **14**, 1238–1241.

Rabinowicz, M., Nicola, A. & Vigneresse, J. 1984 A rolling mill effect in the asthenosphere beneath oceanic spreading centers. *Earth planet. Sci. Lett.* **67**, 97–108.

Ribe, N. 1985 The deformation and compaction of partially molten zones. *Geophys. Jl R. astr. Soc.* **83**, 137–152.

Ribe, N. 1988 On the dynamics of mid-ocean ridges. *J. geophys. Res.* **93**, 429–436.

Ribe, N. & Smooke, M. 1987 A stagnation point flow model for melt extraction from a mantle plume. *J. geophys. Res.* **92**, 6437–6443.

Richter, R. M. & McKenzie, D. 1984 Dynamical models for melt segregation from a deformable matrix. *J. Geol.* **92**, 729–740.

Scheidegger, A. E. 1974 *The physics of flow through porous media*. University of Toronto Press.

Scott, D. 1988 The competition between percolation and circulation in deformable porous medium. *J. geophys. Res.* **93**, 6451–6462.

Scott, D. & Stevenson, D. 1984 Magma solitons. *Geophys. Res. Lett.* **11**, 1161–1164.

Scott, D. & Stevenson, D. 1986 Magma ascent by porous flow. *J. geophys. Res.* **91**, 9283–9296.

Scott, D. & Stevenson, D. 1989 A self-consistent model of melting, magma migration, and buoyancy-driven circulation beneath mid-ocean ridges. *J. geophys. Res.* **94**, 2973–2988.

Scott, D., Stevenson, D. & Whitehead, J. 1986 Observations of solitary waves in a deformable pipe. *Nature, Lond.* **319**, 759–761.

Sotin, C. & Parmentier, E. M. 1989 Dynamic consequences of compositional and thermal density stratification beneath spreading centers. *Geophys. Res. Lett.* **16**, 835–838.

Sparks, D. W. & Parmentier, E. M. 1990*a* 3-D flow beneath spreading centers due to compositional and thermal buoyancy. *Eos, Wash.* **71**, 1637.

Sparks, D. W. & Parmentier, E. M. 1990*b* Buoyant flow beneath ridge-transform systems and along-axis variations in gravity and crustal thickness. *Eos, Wash.* **71**, 627.

Sparks, D. W. & Parmentier, E. M. 1991 Melt extraction from the mantle beneath spreading centers. *Earth planet. Sci. Lett.* **105**, 368–377.

Spiegelman, M. 1991 2-D or not 2-D: understanding melt migration near a sloping, freezing boundary. *Eos, Wash.* **72**, 265.

Spiegelman, M. 1992 Passive vs. active flow? Only the tracers know... *Eos, Wash.* **73**, 290.

Spiegelman, M. 1993*a* Flow in deformable porous media. Part 1. Simple analysis. *J. Fluid Mech.* **247**, 17–38.

Spiegelman, M. 1993*b* Flow in deformable porous media. Part 2. Numerical analysis – the relationship between shock waves and solitary waves. *J. Fluid Mech.* **247**, 39–63.

Spiegelman, M. & McKenzie, D. 1987 Simple 2-D models for melt extraction at mid-ocean ridges and island arcs. *Earth planet. Sci. Lett.* **83**, 137–152.

Toomey, D. R., Purdy, G. M., Solomon, S. C. & Wilcox, W. S. D. 1990 The three-dimensional seismic velocity structure of the East Pacific Rise near latitude 9° 30′ N. *Nature, Lond.* **347**, 639–645.

Von Bargen, N. & Waff, H. S. 1986 Permeabilities, interfacial areas and curvatures of partially molten systems: results of numerical computations of equilibrium microstructures. *J. geophys. Res.* **91**, 9261–9276.

PHILOSOPHICAL TRANSACTIONS OF THE ROYAL SOCIETY A MATHEMATICAL, PHYSICAL & ENGINEERING SCIENCES

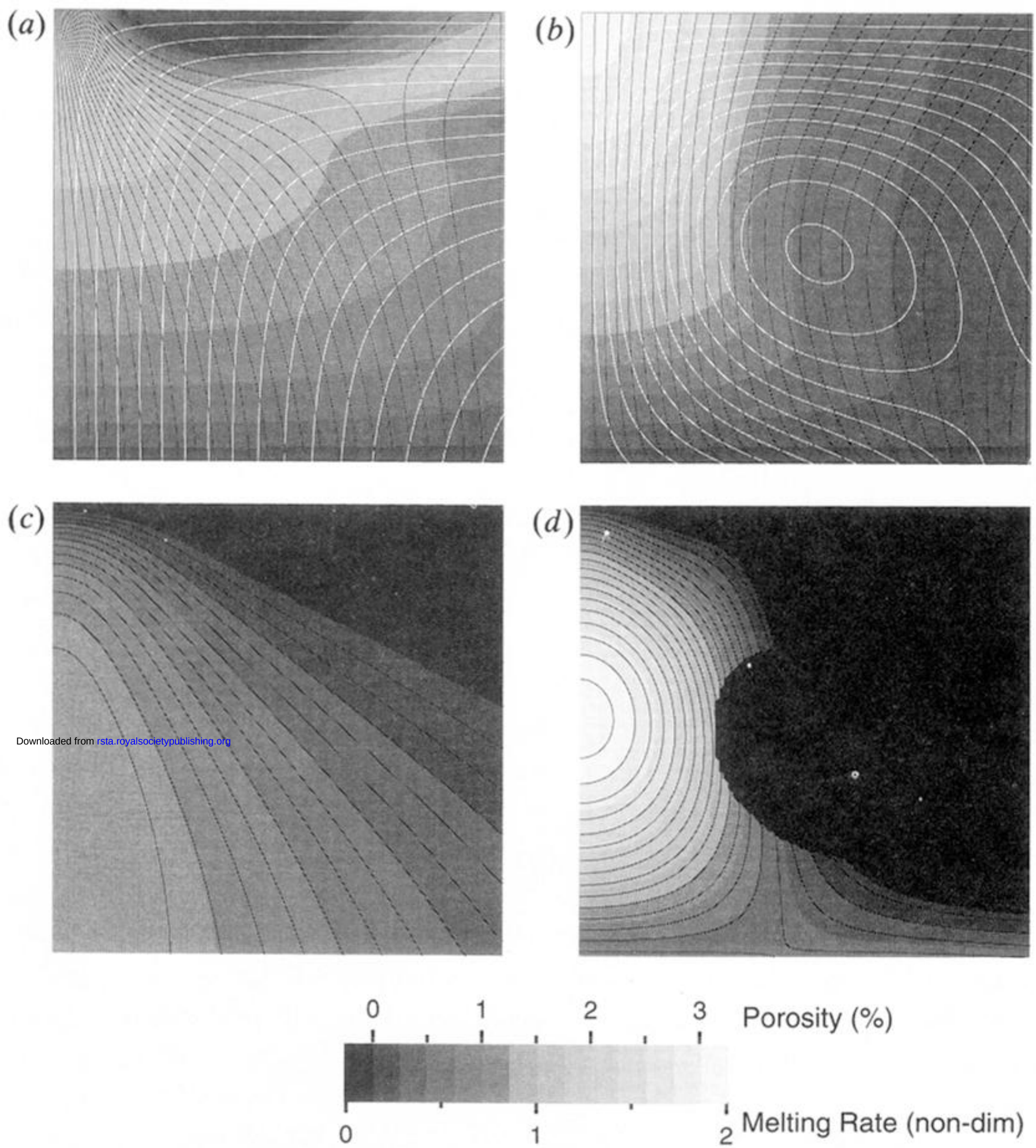

igure 3. 2D solutions for the flow of melt and solid for a simple ridge spreading geometry emonstrating the effects of passive against active mantle flow. The top two parts show porosity, elt flow (black curves) and matrix flow (white curves). The bottom two figures show the mensionless melting rate which is proportional to upwelling rate for 'fertile' upwelling mantle. = 0 on closed streamlines or downwelling regions. Each part shows the right half of the melting gion. The vertical scale is the melting depth (50–60 km) and there is no vertical exaggeration. R related to the Raleigh number and measures the relative contribution of buoyancy forces to scous forces. (*a*) Plate-dominated flow, $R = 0.0357$. When shear is dominated by boundary nditions, the forced shear of the viscous matrix can produce large pressure gradients that focus e flow of melt. (*b*) Buoyancy driven flow, $R = 56.28$. For lower viscosities or plate velocities, uriations in melt content can drive additional small-scale convection which narrows the width of e upwelling region. (*c*) Melting rate field for plate driven shear, (*d*) and for buoyancy driven shear.

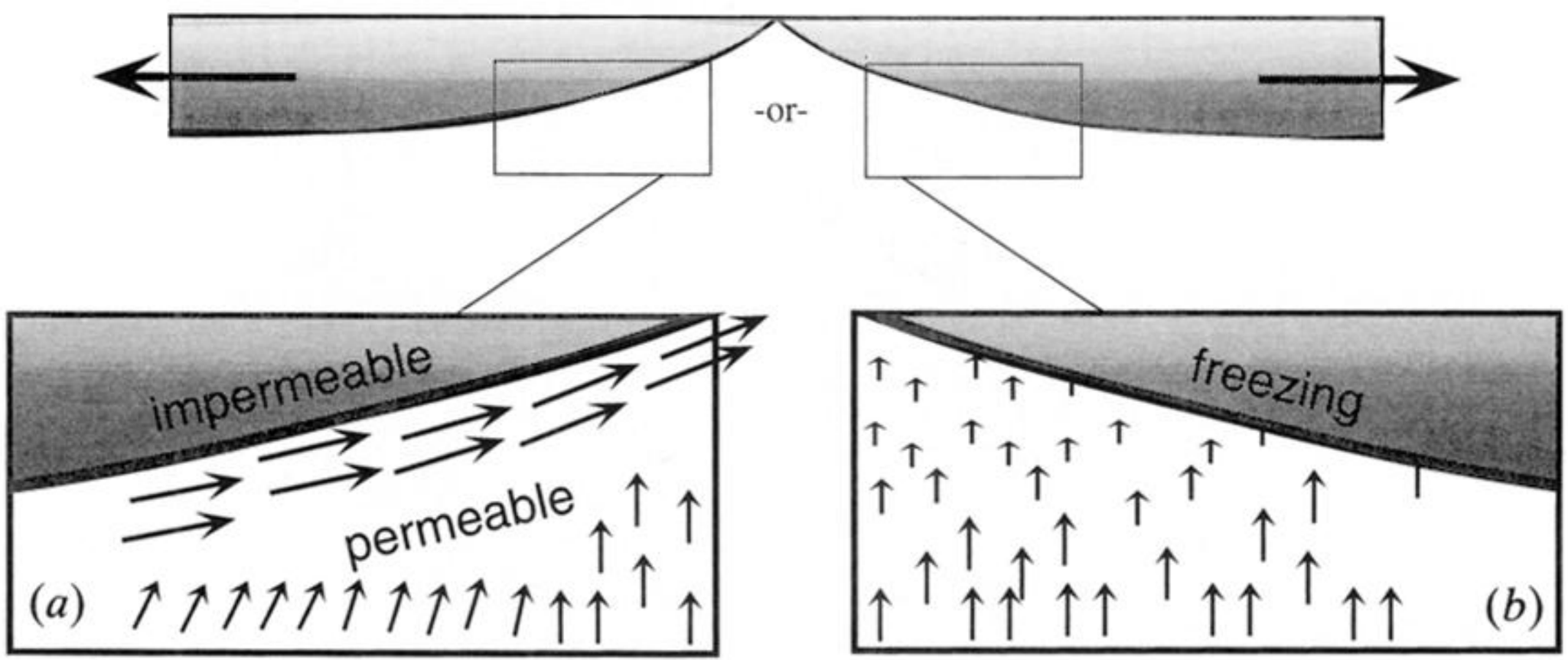

gure 4. The two fundamental effects of freezing on the flow of melt near the top of the partly olten region. (*a*) Melt channelling: because the cooling plates form a natural sloping impermeable rrier to melt flow, channels may arise that transport melt to the ridge axis. (*b*) Simple freezing: melt approaches the freezing boundary, it will be converted to solid which is transported away the spreading plates.

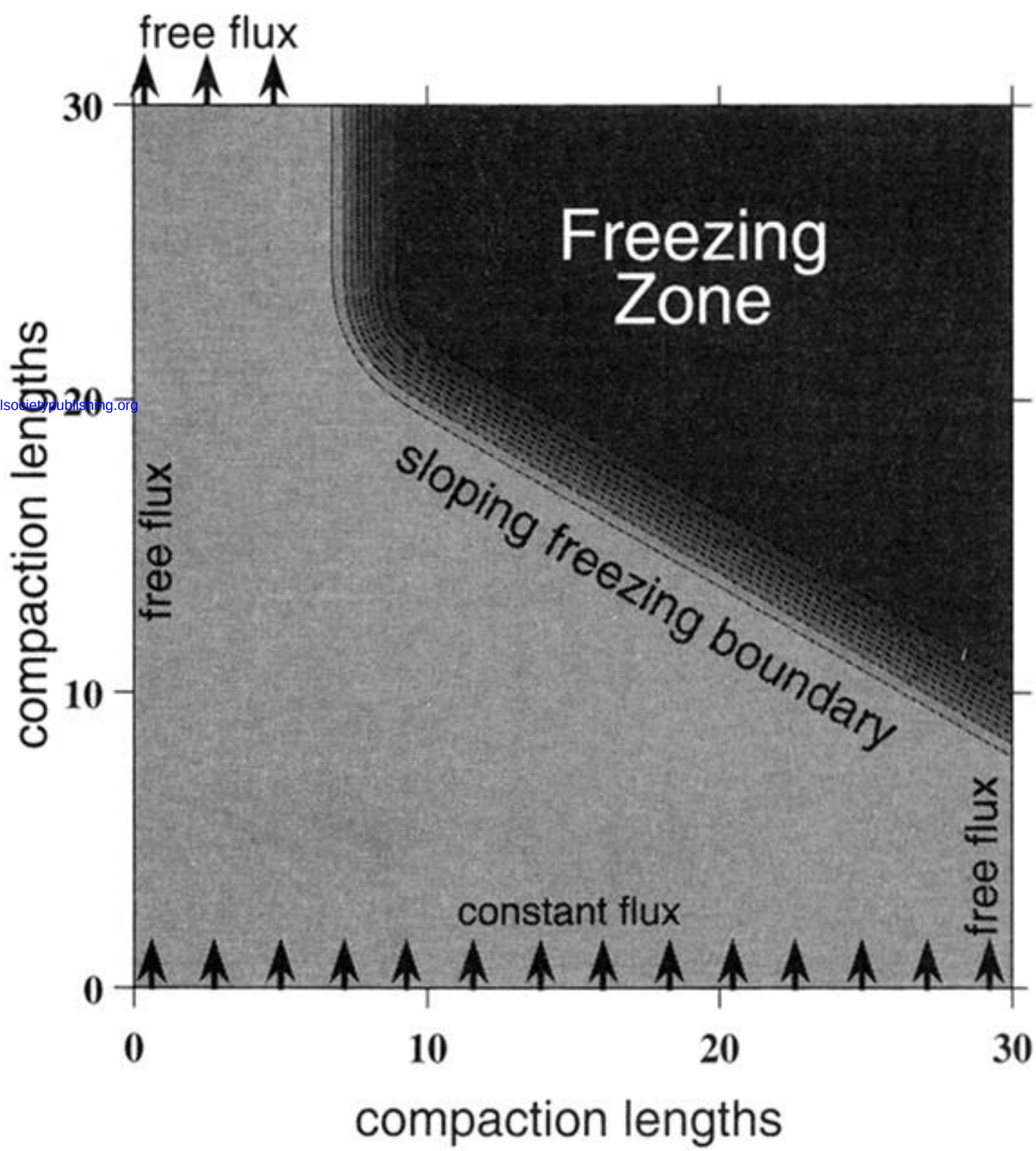

gure 5. Geometry and boundary conditions used to investigate melt migration near a sloping eezing boundary. Freezing occurs in the darker region marked freezing zone. Contours and ading show values of the imposed freezing rate field $\Gamma(\boldsymbol{x})$. The freezing length, $\delta_f = 1/\Gamma_0$ is pproximately the length scale (in compaction lengths) over which a uniform melt flux would freeze mpletely. There is no matrix shear. Boundary conditions are constant melt flux into the base, ee flux out the top and sides. The problem is non-dimensional with length scaled to the mpaction length δ, porosity scaled to the uniform background porosity ϕ_0, and velocities to the ckground melt velocity w_0. Typical values for δ are 100–1000 m, for ϕ_0 are 1–10 % and for w_0 are 1–1 m a^{-1}.

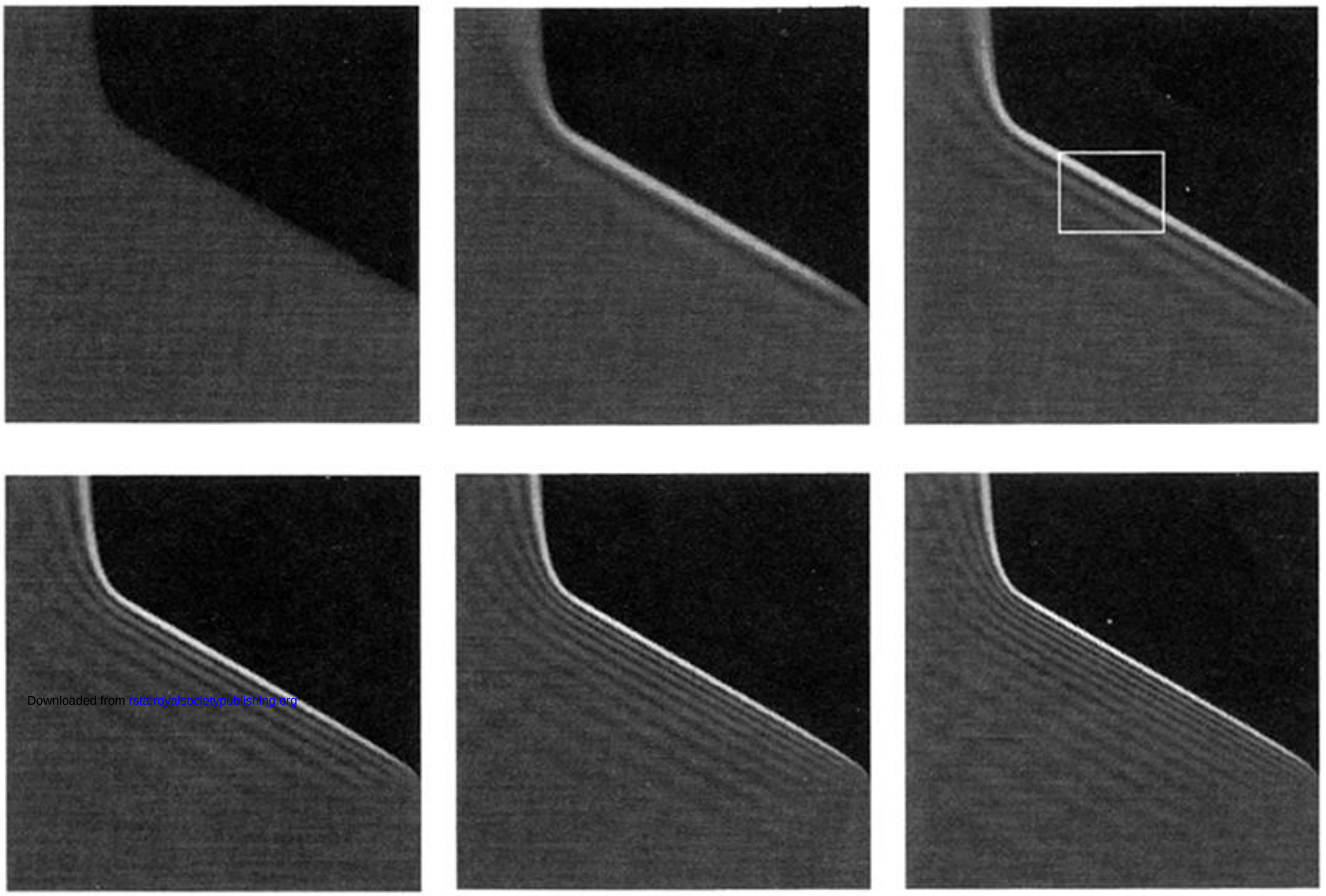

gure 6. Evolution of porosity near a freezing zone with a rapid freezing rate ($\Gamma_0 = -2.0$) showing e development of high permeability melt channels near the freezing boundary. Each box is $\times 30$ compaction lengths on a side and shading shows porosity relative to the background rosity ($\phi = 1$) for dimensionless times $t = 0$, 10, 20 (top row), 40, 60, 80 (bottom row). A mensionless time of 30 is the time required for a completely incompatible trace element to travel ross the box at the background melt velocity. The initial condition is the steady-state solution ven by the zero compaction length approximation where the melt can only percolate vertically d then freeze. At $t = 10$ the excess melt that cannot be accommodated by freezing begins to cumulate at the boundary in a growing channel ($\phi_{\max} \approx 2.4$). With time the initial channel grows a porosity approximately 3.5 times greater than the background. Rather than growing into a ngle channel, however, the growth of each channel initiates the formation of a new channel below in the same manner as the dispersion of solitary waves. The white box at $t = 20$ is the region picted in figure 7*a*.

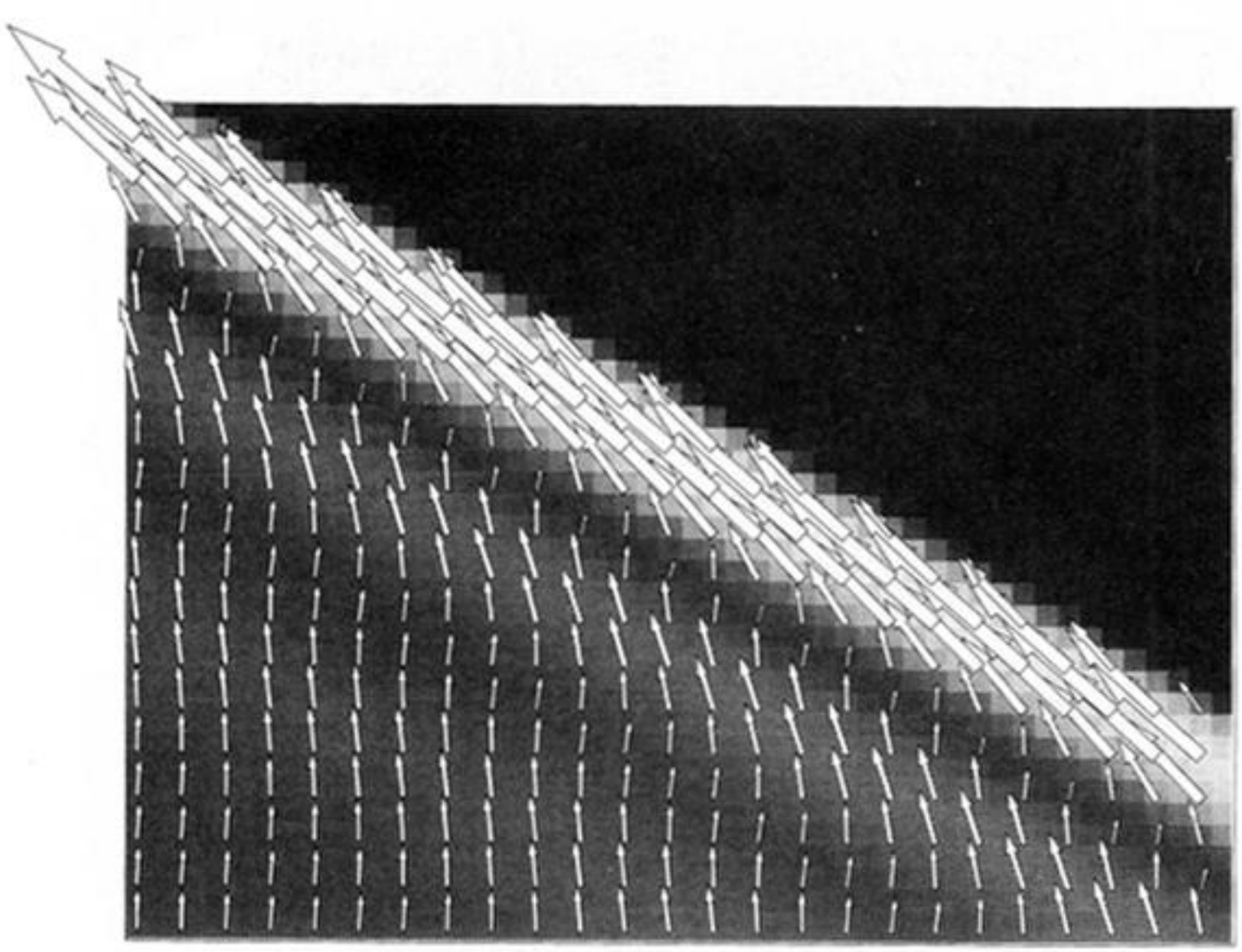

(a)

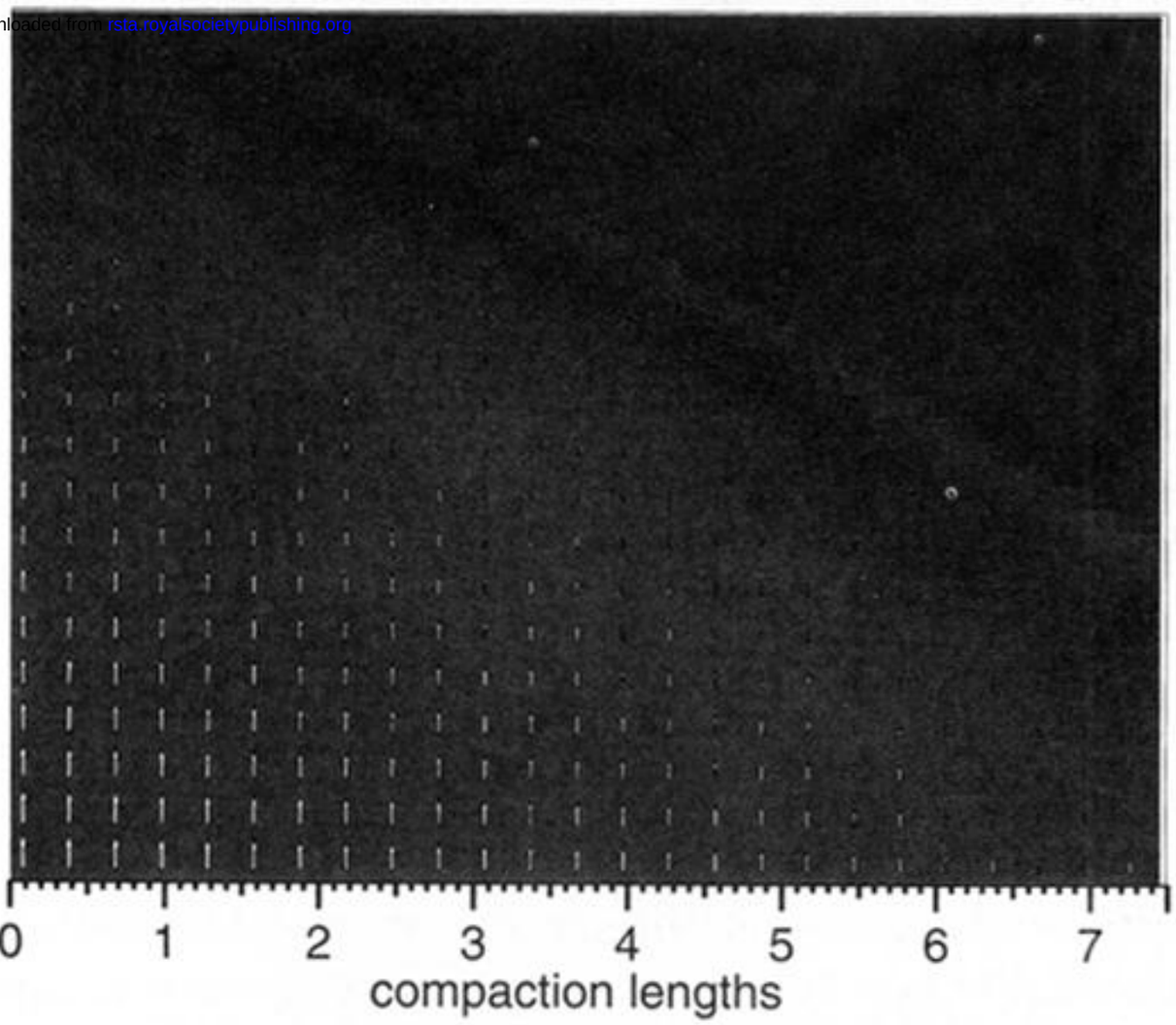

(b)

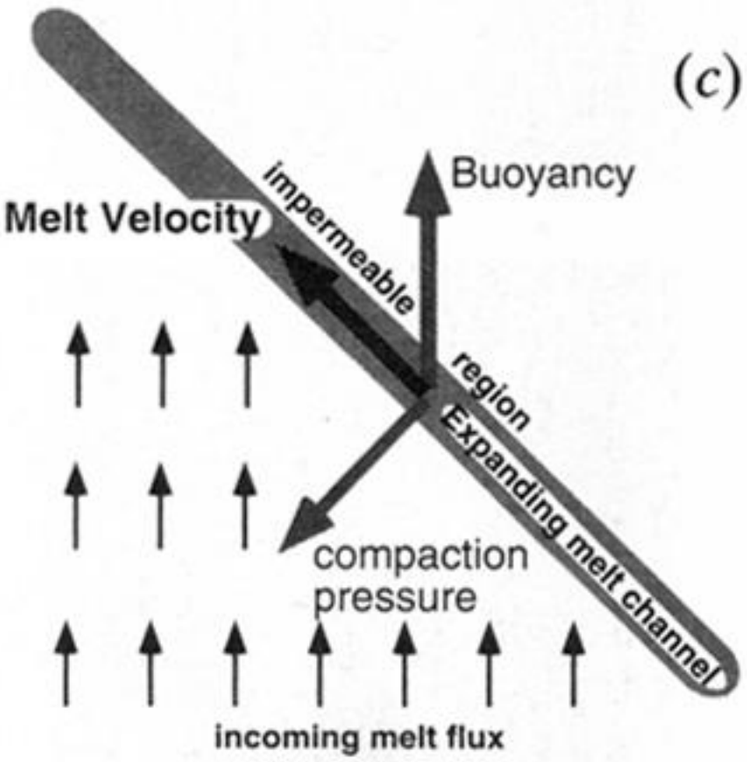

Figure 7. Close-up of the freezing boundary at $t = 20$ showing melt flux vectors for rapid and slow freezing rates. (*a*), (*b*) The 7.5×5.7 compaction length regions marked in figures 6 and 8. (*a*) Rapid freezing rate ($\Gamma_0 = -2.$): This figure shows that not only does the obstruction in flux cause porosity to increase near the freezing boundary, but also that the melt in these channels travels laterally. (*b*) When the freezing rate is slower ($\Gamma_0 = -0.1$), melt only percolates vertically. (*c*) Schematic diagram showing pressure gradients that make the melt flow laterally. When the melt flux is reduced by freezing over many compaction lengths, the compaction pressure is negligible and no channels form.

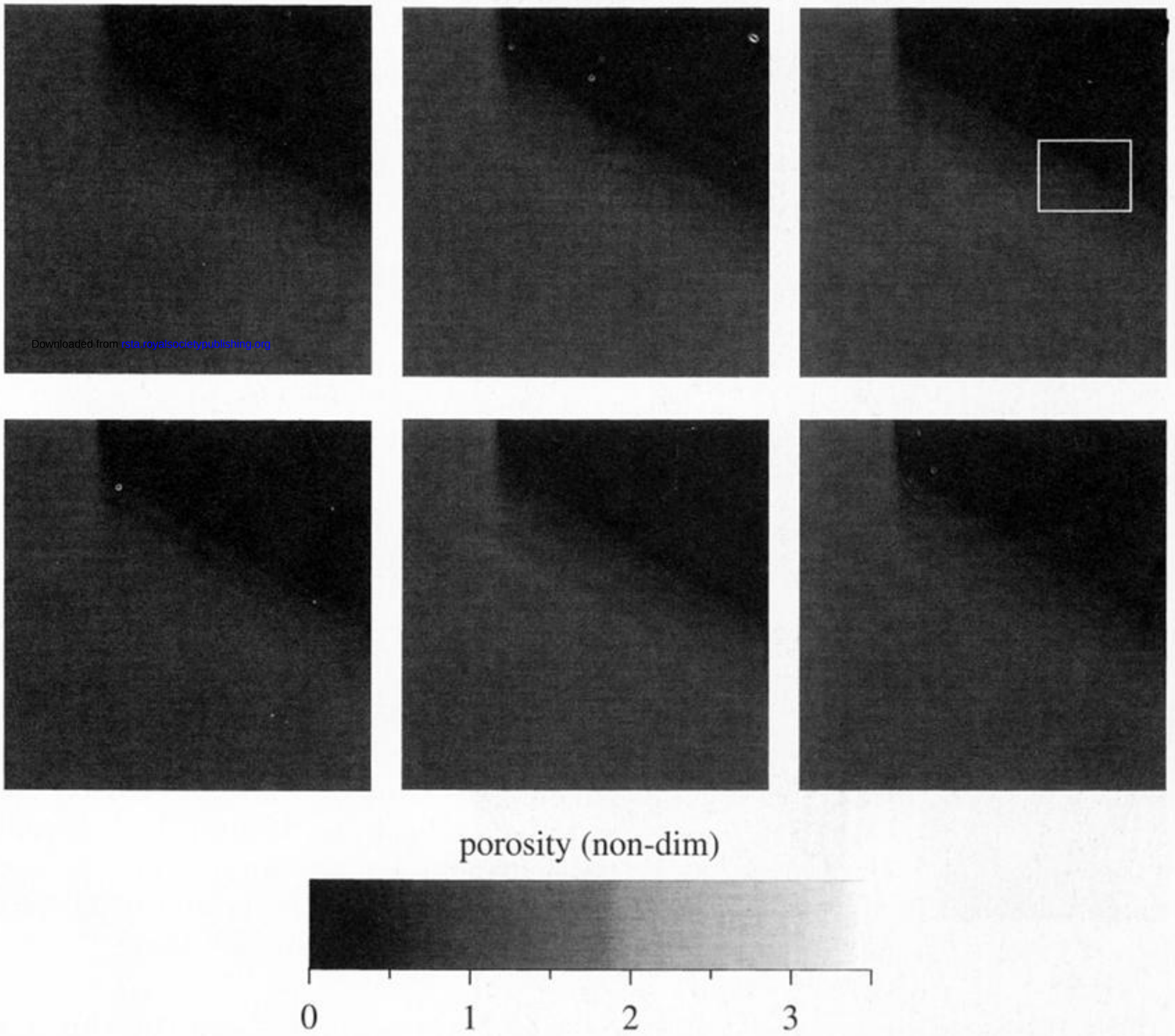

igure 8. Evolution of porosity near a freezing zone with a slow freezing rate $\Gamma_0 = -0.1$ ($t = 0$, 10,) (top row), 40, 60, 80 (bottom row). When freezing occurs over a region that is large compared the compaction length, viscous pressure gradients are negligible and only weak channels form. ith time, this solution develops a weak oscillation that is related to the dispersion of solitary aves (§2c), however, as a first approximation, this solution maintains steady state. The white box ; $t = 20$ is the region depicted in figure 7b.